Electronic Supplementary Material (ESI) for Nanoscale.
This journal is © The Royal Society of Chemistry 2019

Supplementary information

Epitaxial Growth of Dual-Color-Emitting Organic Heterostructures via Binary Solvent Synergism Driven Sequential Crystallization

Baipeng Yin,[a] Jianmin Gu,[a,b,] Man Feng,[a] Guang Cong Zhang,[a] Ziming Zhang,[a] Jinling Zhong,[a] Chuang Zhang,[c] Bin Wen[b,]* and Yong Sheng Zhao[c,]**

[a]Hebei Key Laboratory of Applied Chemistry, School of Environmental and Chemical Engineering, Yanshan University, Qinhuangdao 066004, China.

[b]State Key Laboratory of Metastable Materials Science and Technology (MMST), Yanshan University, Qinhuangdao 066004, China

[c]Key Laboratory of Photochemistry, Institute of Chemistry, Chinese Academy of Sciences, Beijing 100190, China.

E-mail: jmgu@ysu.edu.cn; wenbin@ysu.edu.cn; yszhao@iccas.ac.cn

Contents

i. **Methods.**

ii. **Figure S1.** Room-temperature PL intensities of individual Alq_3 (black) and BPEA (red) solution at different concentrations (C), recorded upon excitation at 365 nm.

iii. **Figure S2.** PL images of dispersed BPEA and Alq_3 nanostructures prepared when ethyl acetate (a), benzene (b) and tetrahydrofuran (c) were used as the anti-solvent, respectively. Scale bar is 250 μm.

iv. **Figure S3.** The high-magnification SEM image of single BH. Scale bar is 10 μm.

v. **Figure S4.** LCFM images of a typical single BH collected from the (a, d) green-light and (b, e) red-light regions and (c, f) the dual-color superposed LCFM images. (BH prepared when isobutanol was used as anti-solvent at 0°C (a-c) or n-butanol was used as anti-solvent at 25°C (d-f)) The scale bars correspond to 30 μm.

vi. **Figure S5.** PL images of BHs prepared when isoamyl alcohol was used as the anti-solvent. Scale bar is 150 μm.

vii. **Figure S6.** (a, b) XRD patterns of various BHs formed by using different anti-solvents.

viii. **Figure S7.** PL spectra of BHs formed using different anti-solvents. The excitation wavelength is 365 nm.

ix. **Figure S8.** PL images of BHs prepared when n-Propanol was used as the anti-solvent. Scale bar is 250 μm.

x. **Figure S9.** PL images of BHs prepared when methanol (a) and ethanol (b) were used as the anti-solvents. Scale bars are 250 μm.

xi. **Figure S10.** (a-c) PL images of BHs prepared at three different molar ratios of Alq_3 to BPEA: (a) 1:2, (b) 1:1 and (c) 2:1. All scale bars are 150 μm.

xii. **Figure S11.** (a, b) PL images of BHs obtained at low temperature (0°C). All scale bars are 150 μm.

xiii. **Figure S12.** Calculated heat of formation for the $CHCl_3$-ROH mixtures.

xiv. **Figure S13.** Solubility of BPEA and Alq_3 molecules in different ratios of C_3H_7OH-$CHCl_3$ mixtures.

xv. **Figure S14.** (a) FLIM images of Alq_3 spindle structures; Scale bar is 30 μm. (b) Corresponding PL decay curves (collection of PL decay time in selected areas), instrumental response functions (scattering from the excitation laser), fitted lifetime curves and residuals of the selected areas.

xvi. **Figure S15.** (a-c) FLIM images of BHs with different Alq_3 microstructure numbers when n-Butanol was used as anti-solvent; Scale bars are 30 μm. (d-f) Corresponding PL decay curves (collection of PL decay time in selected areas), instrumental response functions (scattering from the excitation laser), fitted lifetime curves and residuals of the selected areas.

xvii. **Figure S16.** (a) FLIM images of BHs when 1-Pentanol was used as anti-solvent; Scale bars are 30 μm. (b) Corresponding PL decay curves (collection of PL decay time in selected areas), instrumental response functions (scattering from the excitation laser), fitted lifetime curves and residuals of the selected areas.

Materials. Tris-(8-hydroxyquinoline)aluminium (Alq_3) and 9,10-bis(phenylethynyl)anthracene (BPEA) were purchased from Alfa Aesar, and used without further treatment. The solvents (A.R.) were purchased from Beijing Chemical Agent, Inc.

Synthesis of organic heterostructures. The heterostructures were prepared by using an anti-solvent diffusion method combined solvent evaporation-induced self-assembly method. In a typical experiment, a stock solution containing both Alq_3 (C_{Alq3} = 2, 4 or 8 mM) and BPEA (C_{BPEA} = 4 mM) in $CHCl_3$ was pre-prepared first (C_{Alq3}:C_{BPEA} = 1:2, 1:1 or 2:1). Subsequently, 20 μl of the mixture was dropped onto the precleaned Si substrate in a beaker containing 0.5 ml anti-solvent. (The Si substrate was previously cleaned by sequential ultrasonic rinses in acetone, ethanol and deionized water.) To avoid direct contact between the mixture and anti-solvent, the Si substrate was placed on top of an inner pillar taller than the level of anti-solvent. The beaker was sealed with cap to prevent the solvent from volatilizing quickly due to its relatively low boiling point. As the solvent and anti-solvent volatilized off thoroughly, organic heterostructures have been successfully prepared. The solvent evaporation time varied from 2 h to 12 h, according to the type of anti-solvent.

Synthesis of Alq_3 spindle structures and BPEA microwires. In a typical synthesis, 20 μL of BPEA solution (4 mM) in good solvent of $CHCl_3$, was dropped onto the precleaned Si substrate in a beaker containing 0.5 ml isopropanol. To avoid direct contact between the BPEA solution and anti-solvent, the Si substrate was placed on top of an inner pillar taller than the level of anti-solvent. The beaker was sealed with cap to prevent the solvent from volatilizing quickly. As the solvent and anti-solvent volatilized off thoroughly, BPEA microwires were obtained. Alq_3 spindle structures were also synthesized following the similar experiment procedure.

characterization. The morphology and crystal structure of the as-prepared samples were examined by scanning electron microscopy (SEM, Hitachi S-4800) and X-ray diffraction (XRD, Bruker AXS D8 diffractometer), respectively. The fluorescence microscopy images

were taken with a fluorescence microscope by exciting the samples with the UV band (330-380 nm) of a mercury lamp. The PL spectra were measured with fluorescent spectroscopy (HITACHI F-4500). PL lifetime images were taken with an FLIM setup by scanning the samples with a 375 nm picosecond pulse laser. The FLIM setup (PicoQuant) was made up of picosecond pulsed diode laser (PDL 800-D), fiber coupling unit (FCU II), laser scanning microscope (Olympus FV-1000), four channel detector router (PHR 800), and photomultiplier detector assembly (PMA Series). All spectroscopic and optical measurements were carried out at room temperature.

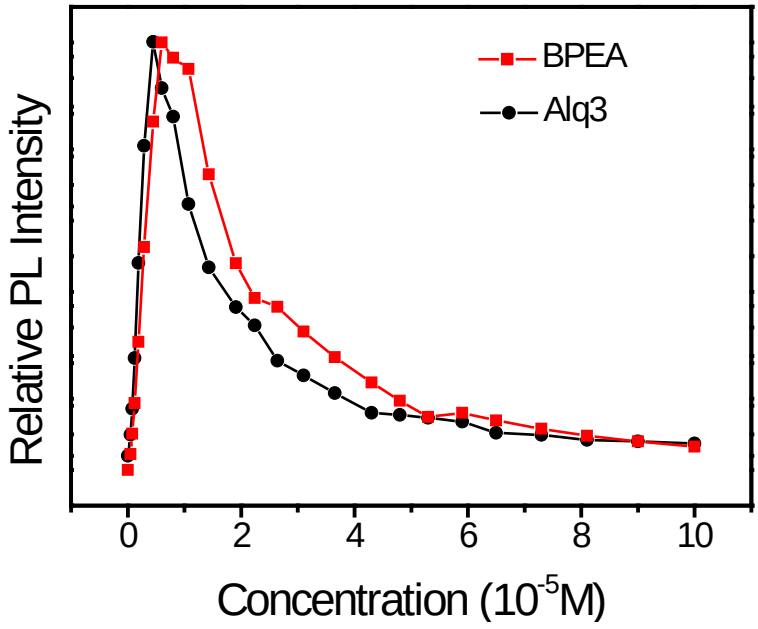

Figure S1. Room-temperature PL intensities of individual Alq_3 (black) and BPEA (red) solution at different concentrations (C), recorded upon excitation at 365 nm.

The intensities of Alq_3 PL (black) increases almost linearly as a function of C until C_{Alq3}= 0.5×10^{-5} M, then drops with increasing the value of C_{Alq3} probably due to the concentration quenching effect. This indicates the formation of Alq_3 aggregation with a threshold concentration of 0.5×10^{-5} M. The threshold concentration of BPEA aggregation is determined to be 0.6×10^{-5} M (red), which is almost the same as that for the formation of Alq_3 aggregation.

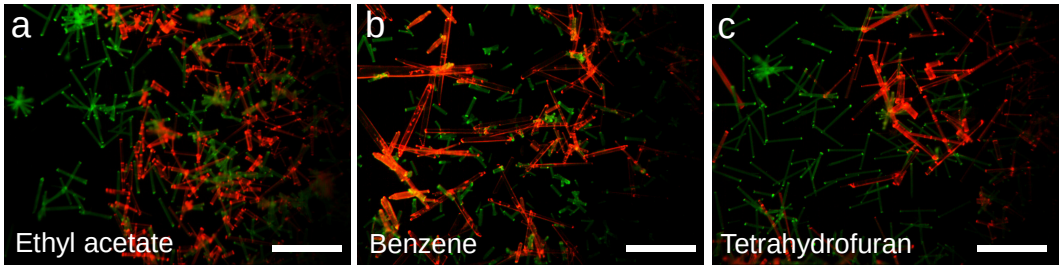

Figure S2. PL images of dispersed BPEA and Alq_3 nanostructures prepared when ethyl acetate (a), benzene (b) and tetrahydrofuran (c) were used as the anti-solvent, respectively. Scale bar is 250 μm.

When non-alcohol solvents were used as the anti-solvent, BPEA and Alq_3 almost simultaneously nucleated and crystallized into dispersed BPEA and Alq_3 nanostructures. (Ethyl acetate (a), benzene (b) and tetrahydrofuran (c))

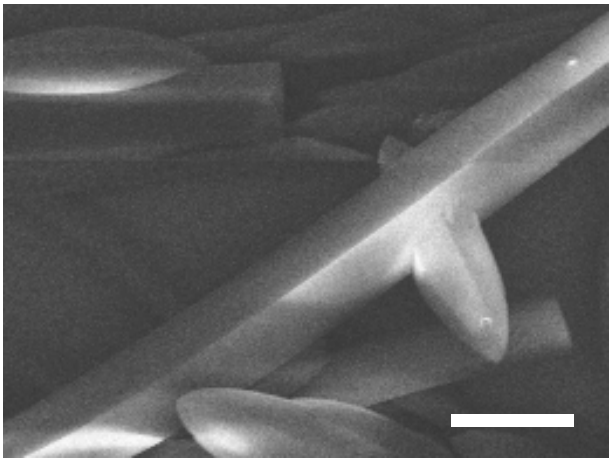

Figure S3. The high-magnification SEM image of single BH. Scale bar is 10 μm.

The high-magnification SEM image indicates each trunk microwire has rectangular cross section.

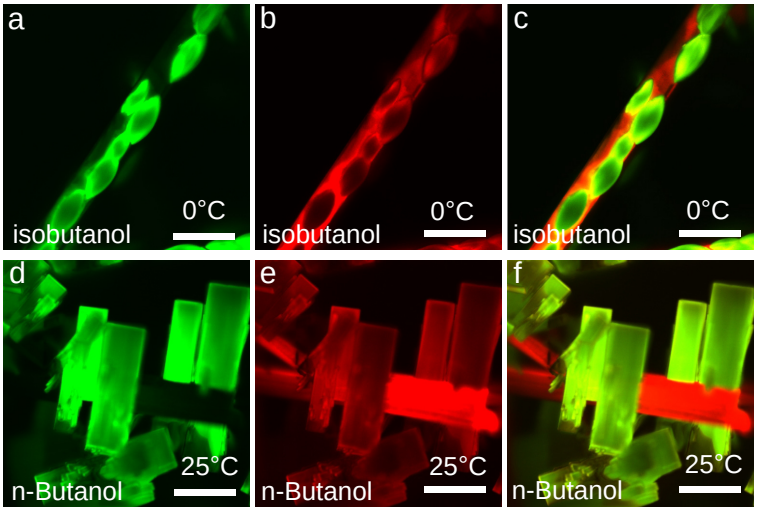

Figure S4. LCFM images of a typical single BH collected from the (a, d) green-light and (b, e) red-light regions and (c, f) the dual-color superposed LCFM images. (BH prepared when isobutanol was used as anti-solvent at 0°C (a-c) or n-butanol was used as anti-solvent at 25°C (d-f)) The scale bars correspond to 30 μm.

LCFM images of a single BH clearly revealed the spatial distribution of Alq_3 and BPEA. In particular, monitored in the red-light region (560-620 nm) showed only a red-emitting segment on the BH body (Figure S3b, e). And monitored in the green-light region (500-560 nm) showed clear emission of bright green light from the microstructure on the microwires surface, whereas the red-emitting body was nearly nonemissive (Figure S3a, d). The superposed LCFM image (Figure S3c, f) also confirms the growth of Alq3 on the BPEA microwires surface.

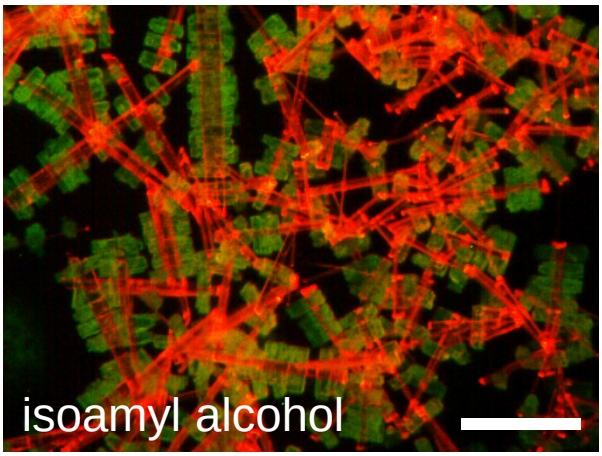

Figure S5. PL images of BHs prepared when isoamyl alcohol was used as the anti-solvent. Scale bar is 150 μm.

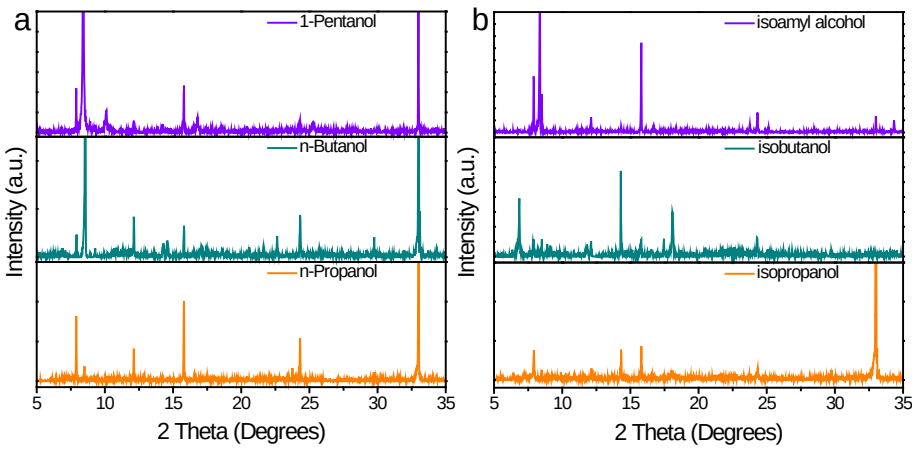

Figure S6. (a, b) XRD patterns of various BHs formed by using different anti-solvents.

XRD patterns of various BHs formed by using different anti-solvents show that the BHs agree well with those of the corresponding α-phase crystals of BPEA and Alq_3. Moreover, it is worth noting that the addition of Alq_3 did not destroy the original crystal structure of the seed microwires.

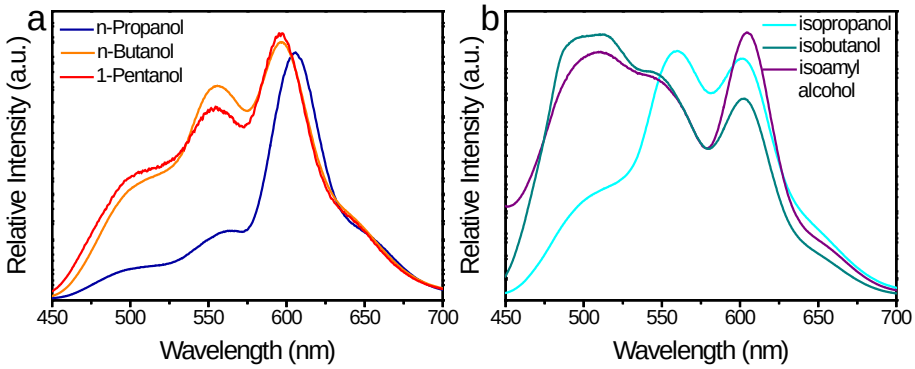

Figure S7. PL spectra of BHs formed using different anti-solvents. The excitation wavelength is 365 nm.

To investigate the effect of Alq_3 growth on the optical properties of the seed microwires, PL measurements were carried out. The PL spectrum of the various BHs consists of a peak at 560 nm and 601 nm due to the BPEA component and another peak at 512 nm due to the Alq_3 component. However, the PL spectrum of the BHs is not a simple mixture or sum of the individual PL spectra of the component because the emission from BPEA is so relative to that of Alq_3. The relatively intense BPEA PL (560 nm) indicates efficient direct energy transfer from Alq_3 to BPEA the heterojunction interface because of the good overlap of the excitation spectrum of BPEA with the emission spectrum of Alq_3.

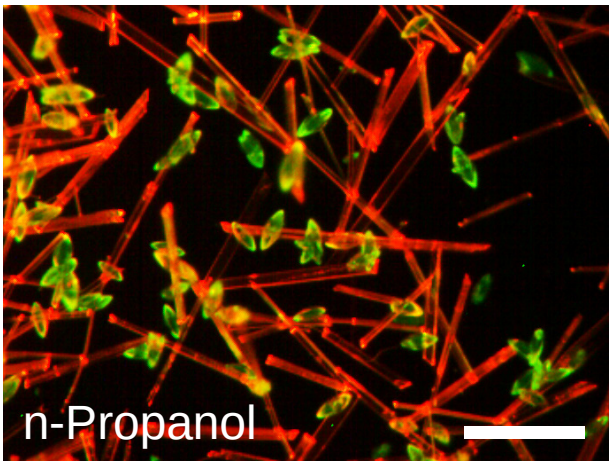

Figure S8. PL images of BHs prepared when n-Propanol was used as the anti-solvent. Scale bar is 250 μm.

When n-Propanol was used as the anti-solvent, the heterojunctions obtained is similar to that of isopropanol or isobutanol as an anti-solvent, but it has a poorer degree of aggregation than the BHs described above.

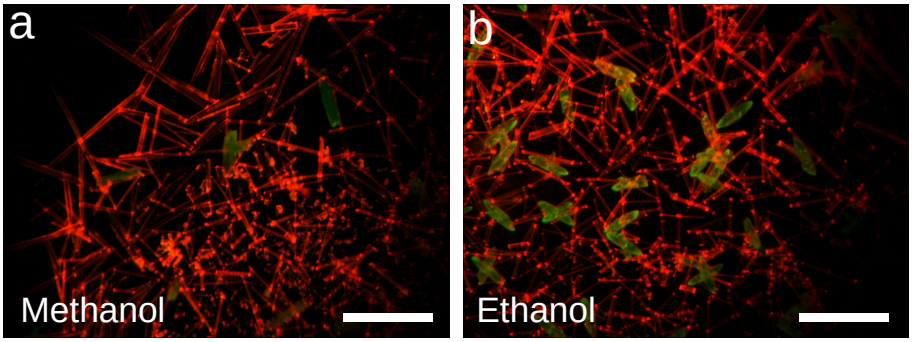

Figure S9. PL images of BHs prepared when methanol (a) and ethanol (b) were used as the anti-solvents. Scale bars are 250 μm.

When methanol or ethanol was used as anti-solvents, only the presence of BPEA microwires was observed in the sample because the lower chain length alcohols were detrimental to the crystallization of Alq_3.

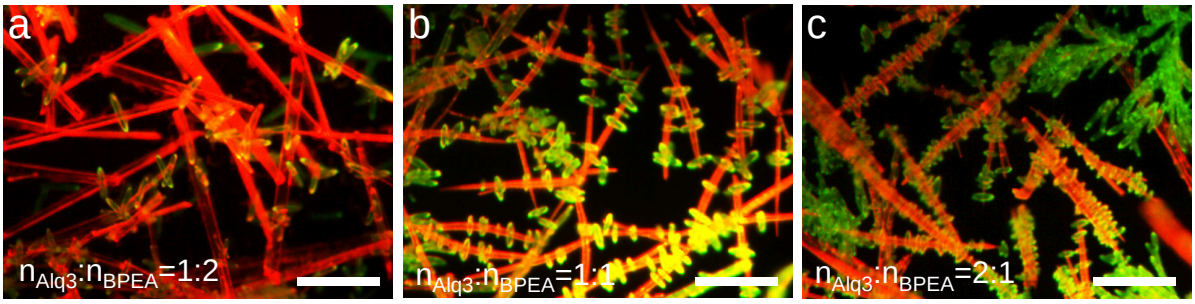

Figure S10. (a-c) PL images of BHs prepared at three different molar ratios of Alq_3 to BPEA: (a) 1:2, (b) 1:1 and (c) 2:1. All scale bars are 150 μm.

In order to fine-tune the BHs, the number of Alq_3 microstructures needs to be controlled by systematically adjusting the molar ratio of Alq_3 to BPEA. If C_{BPEA} was fixed at 4 mM, when the C_{Alq3} increased from 2 to 4 and to 8 mM, the amount of Alq_3 microstructures deposited on the surfaces of the BPEA microwires can be effectively tuned from several to several dozen.

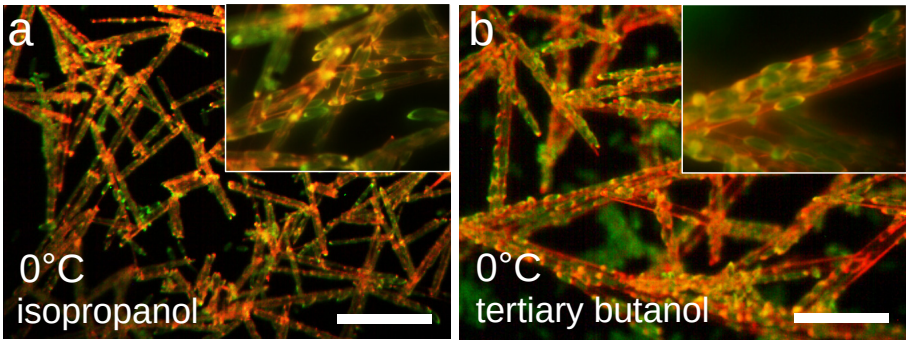

Figure S11. (a, b) PL images of BHs obtained at low temperature (0°C). All scale bars are 150 μm.

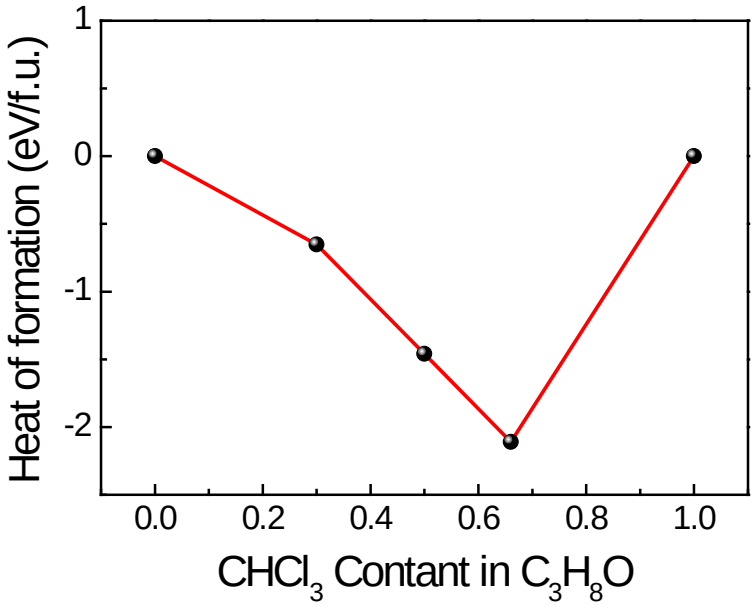

Figure S12. Calculated heat of formation for the $CHCl_3$-ROH mixtures.

The first-principles calculations have been performed within the framework of electronic density functional theory (DFT), as implemented in the Vienne Ab initio Simulation Package (VASP). The exchange and correlation interaction was described by the generalized gradient approximation (GGA) with the Perdewe-Wang (PW91) parameterization. The interactions between ions and valence electrons were modeled by the projector-augmented wave (PAW) method. A plain wave cutoff energy for 500 eV has been used. Brillouin zone integrations were modeled by using Gama point. The heats of formation for mixing $CHCl_3$ and C_3H_7OH (isopropanol) with different ratio can be obtained from the following formula:

$$E_{from}^{CHCl_3-C_3H_7OH} = \left[E_{total}^{CHCl_3-C_3H_7OH} - (aE^{CHCl_3} + bE^{C_3H_7OH})\right]/(a+b)$$

Negative heat of formation for mixing $CHCl_3$ and C_3H_7OH show a strong interaction when mixing alcohols anti-solvent with $CHCl_3$ solvent, indicating that there exist a stable $CHCl_3$-ROH complex in the mixing solvent.

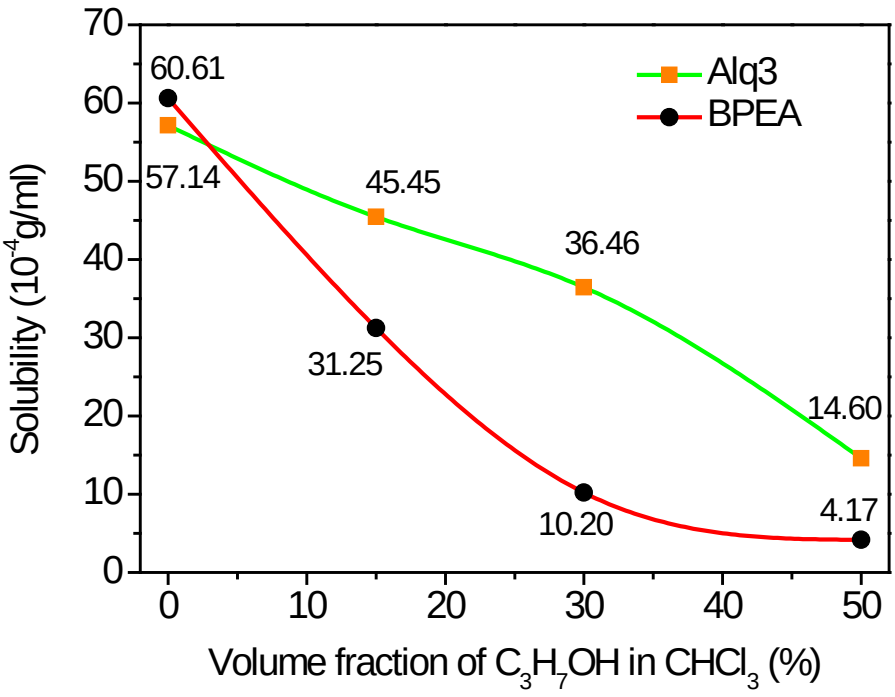

Figure S13. Solubility of BPEA and Alq_3 molecules in different ratios of C_3H_7OH-$CHCl_3$ mixtures.

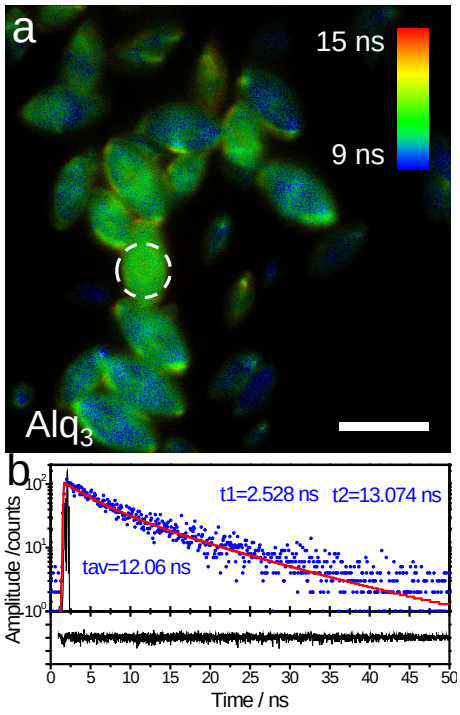

Figure S14. (a) FLIM images of Alq_3 spindle structures; Scale bar is 30 μm. (b) Corresponding PL decay curves (collection of PL decay time in selected areas), instrumental response functions (scattering from the excitation laser), fitted lifetime curves and residuals of the selected areas.

In the absence of BPEA energy acceptor, the PL lifetime of Alq_3 was 12.06 ns, revealing the intrinsic exciton lifetime of Alq_3 without extrinsic PL quenching.

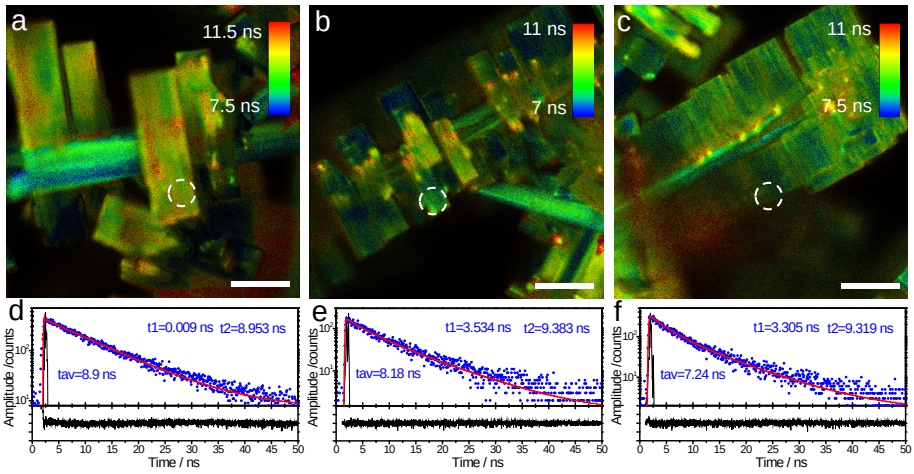

Figure S15. (a-c) FLIM images of BHs with different Alq_3 microstructure numbers when n-Butanol was used as anti-solvent; Scale bars are 30 μm. (d-f) Corresponding PL decay curves (collection of PL decay time in selected areas), instrumental response functions (scattering from the excitation laser), fitted lifetime curves and residuals of the selected areas.

The sharp shortening of the Alq_3 lifetime in the heterostructures prove the FRET process from Alq_3 to the BPEA acceptor molecules.

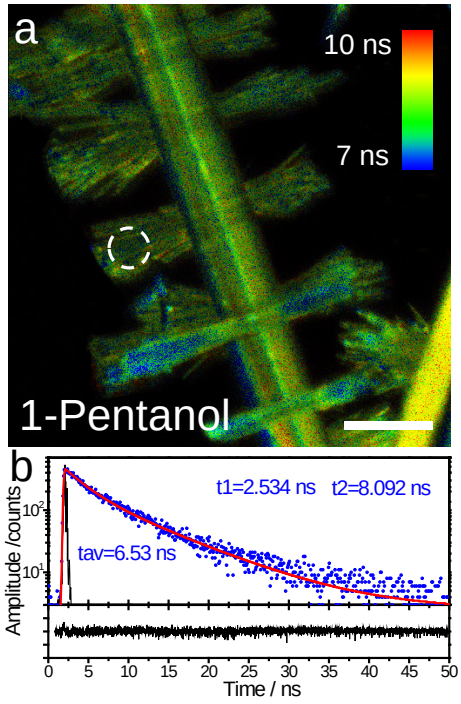

Figure S16. (a) FLIM images of BHs when 1-Pentanol was used as anti-solvent; Scale bars are 30 μm. (b) Corresponding PL decay curves (collection of PL decay time in selected areas), instrumental response functions (scattering from the excitation laser), fitted lifetime curves and residuals of the selected areas.

The sharp shortening of the Alq_3 lifetime in the heterostructures prove the FRET process from Alq_3 to the BPEA acceptor molecules.